

ANALYSIS OF INTEGRATED-LIGHT SPECTRA OF GALACTIC GLOBULAR CLUSTERS

M. E. Sharina,^{1,*} V. V. Shimansky,² and N. N. Shimanskaya²

¹*Special Astrophysical Observatory, Russian Academy of Sciences, Nizhnii Arkhyz, 369167 Russia*

²*Kazan Federal University, Kazan, 420008, Russia*

We present the results of determination of the age, helium mass fraction (Y) in terms of the used stellar evolutionary models, metallicity ($[\text{Fe}/\text{H}]$), and abundances of the elements C, O, Na, Mg, Ca, Ti, Cr and Mn for 26 globular clusters of the Galaxy. In this work, we apply a method developed by us that employs medium-resolution integrated-light spectra of globular clusters and models of stellar atmospheres and it is supplemented in this paper by the automatic calculation of microturbulence velocities of stars in the studied objects. Based on the data obtained for 26 objects, as well as on the results of our previous studies, it is shown that the abundances of chemical elements, that we measured, with the exception of carbon, are consistent with the literature estimates from the analysis of integrated-light spectra of clusters and from high-resolution spectroscopic observations of their brightest stars. Our estimates of $[\text{C}/\text{Fe}]$ are consistent with the literature values obtained from the integrated-light spectra of clusters. We interpret the systematic difference between the derived $[\text{C}/\text{Fe}]$ for globular clusters and the literature $[\text{C}/\text{Fe}]$ values for the brightest stars of the clusters as a change of the chemical composition in the atmospheres of stars during their evolution. The estimated absolute ages and average Y for the clusters are in a reasonable agreement with the literature data from the analysis of color–magnitude diagrams of the objects.

1. INTRODUCTION

The properties of stellar populations of globular clusters have always served as the basis for stellar evolutionary theories (Carney, 2001; Kruijssen et al., 2019). However, despite the progress in observational and theoretical astrophysics, the determination of the absolute ages of globular clusters and helium content in their stars remains a problem (see e.g. Charbonnel, 2016). A particular difficulty is associated with the ex-

planation of the phenomena of multiple stellar populations in globular clusters (Gratton et al., 2012). Abundance anomalies of C, N, O, Na, Al, Mg vary significantly from object to object. The feature common for many globular clusters is the presence of anti-correlations in the abundances of light elements C–N, Na–O, Mg–Al. In some massive globular clusters, stellar populations with different abundances of r -process elements were found. The difficulty in explaining these phenomena lies in the fact that the changes in the elemental abundances that occur during

* Electronic address: sme@sao.ru

the evolution of cluster stars are superimposed on the anomalies of the primary chemical contents, which apparently existed at the time of cluster formation (Kraft, 1994; Charbonnel, 2016 and references therein). Therefore, it is important to study integrated-light spectra of star clusters in order to evaluate how chemical peculiarities influence the properties of the total radiation of objects. First of all, it is necessary to study precisely the globular clusters of our Galaxy, for which there are data from deep stellar photometry and high-resolution spectroscopy of individual stars.

2. OBJECT SAMPLE

Our sample is mainly composed of the globular clusters with integrated-light spectra from the library of Schiavon et al. (2005). These authors used the following method of observations. They drifted the spectrograph slit across the core diameter of the cluster. The sky background spectra were obtained in a similar way outside the boundaries of the clusters. The typical size of the background area was $5'-10'$. For the objects NGC 6205 and NGC 7006, we used the archival data obtained with the CARELEC spectrograph at the 1.93-m telescope in the Haute-Provence Observatory. Instrumental conditions during these observations and methods of data analysis were described in detail in our previous papers: Sharina et al. (2013), Khamidullina et al. (2014) and Sharina et al. (2018). The seeing

was $2''-3''$ during the observations of NGC 6205 and NGC 7006 (July 9–10, 2010). The spectra of NGC 6205 and NGC 7006 were obtained using fixed slit positions, i.e. without drifting the spectrograph slit. For NGC 6205, the observations were carried out using one slit position near the cluster center and oriented along the sky meridian (slit position angle $PA = 0$). The exposure time was 300 s. The sky background exposure was taken outside the cluster boundaries with $PA = 0$. For NGC 7006, one exposure of 900 s. was taken with $PA = 0$. Since the cluster has a visible diameter of approximately $2'$, the regions of the obtained spectrum above and below the object were used to subtract the background.

In this paper, ages, helium mass fraction Y , metallicity $[Fe/H]$ and elemental abundances are determined for 26 clusters. It will be shown in Section 3.1 that the procedure of the automatic accounting for microturbulence velocities developed in this study does not significantly change the results obtained by us earlier with fixed values of this parameter. Therefore, we combine the results of the studies of the globular clusters in the Galaxy from our previous articles with the data obtained in this paper to demonstrate the accuracy of the aforementioned parameters determination taking the advantage of a large object sample. We use the previous results for the following objects: NGC 2419 (Sharina et al., 2013), NGC 6229, NGC 6779, NGC 5904 (Khamidullina et al. 2014), NGC 1904, NGC 5286, NGC 6254,

NGC 6752 and NGC 7089 (Sharina et al., 2017), NGC 104, NGC 6838, NGC 6121, NGC 6341 and NGC 7078 (Sharina et al. 2018). In total, we analyze the results for 40 objects in Section 4.4. Note that the chemical abundances were changed due to the improvement of the method of ξ_{turb} determination for the objects NGC 1851, NGC 2298, NGC 3201, NGC 6218, NGC 6342, NGC 6522, NGC 6624 studied in the above mentioned previous papers. We make a comparison of our results with the following literature values: (1) determination of ages and metallicities of clusters with their color-magnitude diagrams, (2) determination of metallicities and chemical abundances by Conroy et al. (2018) who used integrated-light spectra of Galactic globular clusters from the library of Schiavon et al. (2005), as well as 3) high resolution spectroscopic abundances determination.

3. METHOD

The method of our analysis is described in detail in the papers: Khamidullina et al. (2014); Sharina et al. (2014); Sharina and Shimansky (2020); Sharina et al. (2013, 2018, 2017). In the paper by Sharina et al. (2017), spectra of extragalactic clusters were analyzed with it for the first time. Let us remind the main details of the method. We analyze integrated-light spectra of globular clusters using models of stellar atmospheres for the determination of ages, helium mass fraction Y , metallicity $[\text{Fe}/\text{H}]$, and chemical

abundances in the studied objects. We calculate synthetic spectra based on the plane parallel hydrostatic models of stellar atmospheres (Castelli and Kurucz 2003). Atomic and molecular spectroscopic line lists were taken from the website of R. L. Kurucz (<http://kurucz.harvard.edu/linelists.html>). The atmospheric parameters are determined from stellar evolutionary isochrones, and the calculated synthetic spectra of individual stars are summed according to a certain mass stellar function. In this work, we calculate synthetic spectra in the approximation of the local thermodynamic equilibrium (LTE) and use the isochrones by Bertelli et al. (2008) and stellar mass function by Chabrier (2005).

A comparison of the shapes and intensities of the observed and model absorption lines of the Balmer series of hydrogen and the intensities of the Ca I 4227, and K, and H Ca II 3933.7 Å, and 3968.5 Å lines¹ makes it possible to determine the isochrone that best reproduces the observed spectrum. The temperature of Main sequence (MS) turnoff stars increases with the decreasing age. At the same time, the depths of the cores and wings of hydrogen lines increase. The growth of Y leads to the increase in the mean luminosity and temperature of horizontal branch (HB) stars. The intensities and widths of the hydrogen lines demonstrate the maximum dependency on the stellar luminosity for the stars of type A0 ($8700 \leq T_{\text{eff}} \leq 11\,000$ K). The fur-

¹ The line He contributes the H Ca II line.

ther growth of temperature and luminosity leads to the weakening of the hydrogen lines due to the intense ionization of hydrogen. This process develops rather slowly, since the decrease in absorption coefficients in the Balmer hydrogen lines is partially compensated by a decrease in opacity in the surrounding Paschen continuum.

When metallicity, age and Y change, the depths of the nuclei and wings of each of the hydrogen lines $H\delta$, $H\gamma$, and $H\beta$ change in their own way due to the differences in the contribution of stars of various luminosities and spectral classes depending on the wavelength. This fact allows one to confidently determine the metallicity, age and Y . The Ca I/Ca II ionization balance, discussed above, depends on the temperature and density of the medium. Therefore, this balance is an important additional control indicator that allows one to check the parameters obtained from the hydrogen lines and refine them if necessary.

Since atmospheric parameters are based on stellar evolution isochrones, it is important to verify, for the method evaluation purposes, whether the stellar evolution models selected by analyzing the integrated light spectra from clusters correspond to the observed position of the stars in the color-magnitude diagrams (CMD) of these objects. This task has been carried out for all studied Galactic clusters. We described the methods of CMD analysis in the paper by Khamidullina et al. (2014). Since we know metallicity, age and Y of a cluster from the analysis of its spectrum, during the

isochrones fitting process, we only need to choose the distance to a given object and color excess $E(B - V)$ from Galactic color extinction maps (Schlegel et al., 1998). In order to test our method, Khamidullina et al. (2014) also solved the problem of selecting the following five parameters using CMD: metallicity, age, Y , $E(B - V)$ and distance to the cluster. However, in this paper, this approach is not applied.

To summarize, in this article we present the results of modeling the integrated light spectra of 26 Galactic globular clusters and compare the results with literature values. The main goal of this investigation in the framework of our study is further improvement of our method. Compared to our previous works, we take a new approach to calculating ξ_{turb} .

3.1. Microturbulence velocity

In our previous studies of integrated-light spectra of globular clusters (Khamidullina et al., 2014; Sharina et al., 2014, 2013, 2018, 2017), the same microturbulence velocity value was set for all cluster stars based on the best agreement between theoretical and observational data. However, this approach is a priori incorrect, because ξ_{turb} values vary in a wide range for cluster stars with different stellar parameters. Therefore, we have developed and implemented a method for automatic selection of ξ_{turb} values when calculating synthetic spectra of stars. The aim is to take into account their real variations in clus-

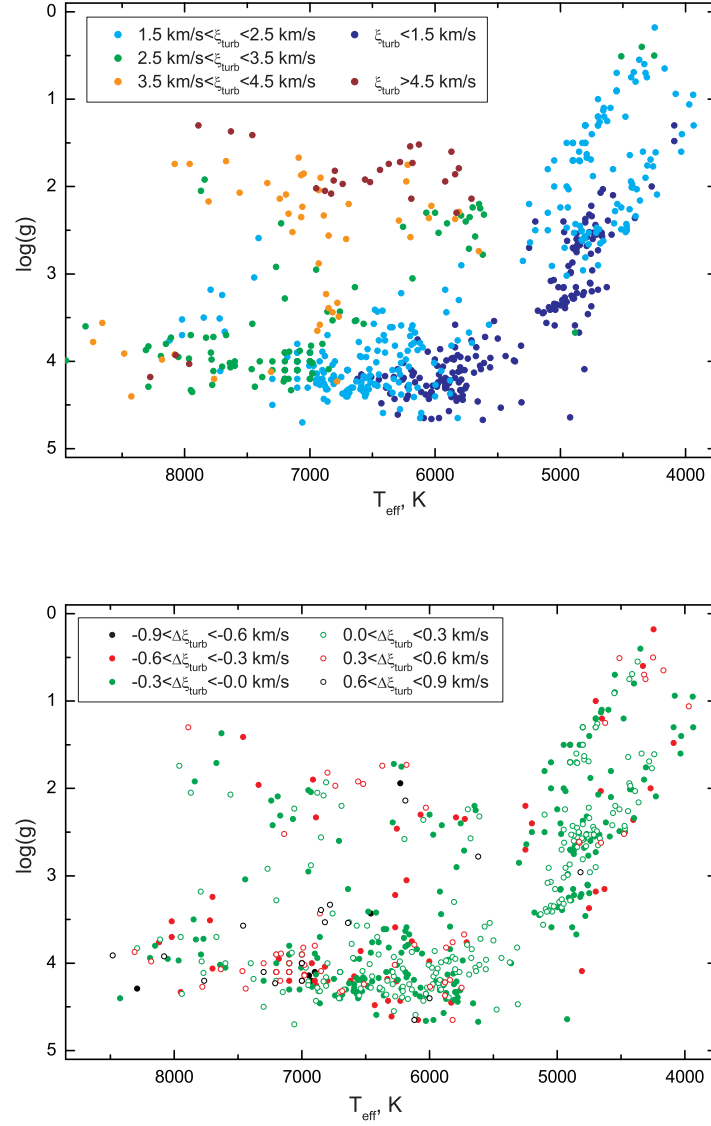


Figure 1. Panel (a): the distribution of 637 stars of the sample in the plane $T_{\text{eff}}\text{--}\log g$. The intervals of ξ_{turb} are indicated where the objects lie. Panel (b): the distribution of 607 stars left after the selection procedure in the plane $T_{\text{eff}}\text{--}\log g$ (see Section 3.1). These stars were used to build the function 1 (see also Table 1). The deviation intervals of the calculated ξ_{turb} from the corresponding literature values are indicated.

ters and reduce the number of free parameters in the analysis of integrated-light spectra. Within the framework of this technique, the functional dependence of ξ_{turb} on the following main parameters of stellar atmospheres is built: the effective temperature T_{eff} and the gravity on the stellar surface $\log g$. For the function building, the observational parameters of stars from the literature were used. In the analyzed sample for parameter ranges, we included 637 objects from complex spectroscopic studies of stars (Bruntt et al., 2012; Kahraman AlicavEes et al., 2016; Men-

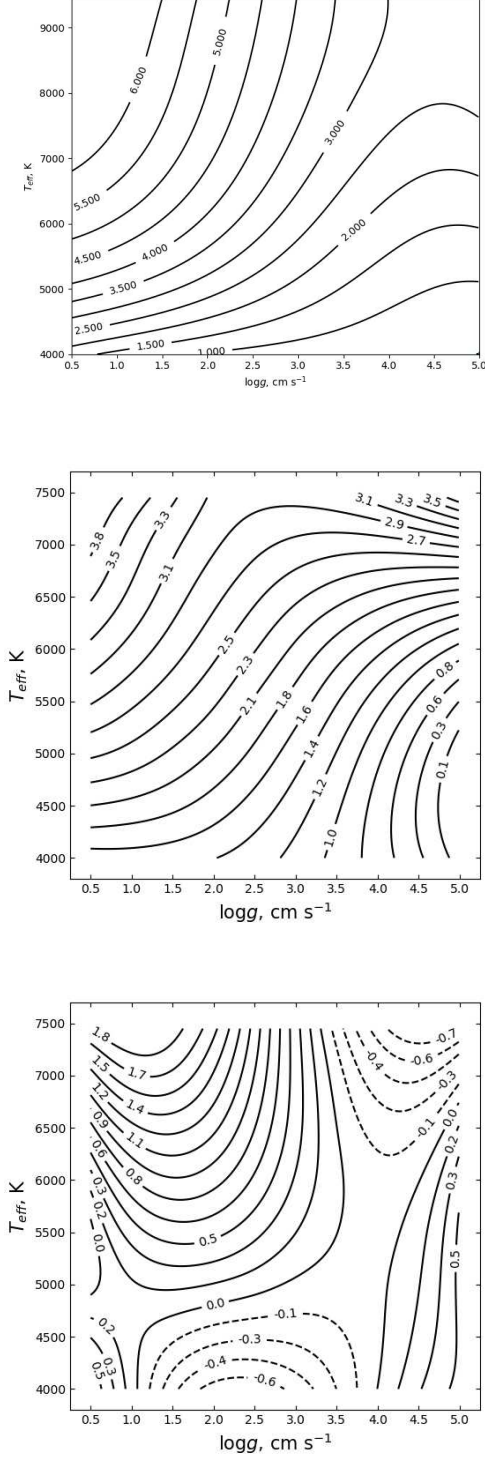


Figure 2. Comparison of the distributions of ξ_{turb} values obtained by us and Boeche and Grebel (2016) in contours on the plane $T_{\text{eff}} - \log g$.

Panel (a): the distribution of the ξ_{turb} values obtained using the function (1). Panel (b): the distribution of the Boeche and Grebel (2016) ξ_{turb} values. Panel (c): the difference in km s^{-1} ($\Delta\xi_{\text{turb}}$) between ξ_{turb} values obtained by us and Boeche and Grebel (2016). Contours with

zhevitski et al., 2014; Santos et al., 2013; Schaefele et al., 2015) where microturbulence velocities were derived from the analysis of FeI and FeII lines using the model atmospheres method and satisfying the standard condition that there should be no dependence between the iron abundance on the equivalent widths of individual lines. The ξ_{turb} values obtained in the literature using different methods did not show significant differences for stars of the same spectral class. Furthermore, it turned out that the functional dependence of ξ_{turb} on T_{eff} and $\log g$ is smooth during the transition from one spectral class to another, which allowed describing it by a third-degree polynomial:

$$\xi_{\text{poly}} = \sum_{i,j=0}^3 a_{ij} \left(\frac{T_{\text{eff}}}{1000 \text{ K}} \right)^i (\log g)^j, \quad (1)$$

where the coefficients calculated using the least squares method are presented in Table 1. A similar relationship was built by Boeche et al. (2011), but for a narrower range of the parameters T_{eff} and ξ_{turb} . The approximation of the observed data in Boeche et al. (2011) was performed by a second-degree polynomial function taking into account all the cross components. Earlier, Boeche et al. (2011) constructed the function of ξ_{turb} versus T_{eff} and $\log g$ using a third-degree polynomial. To our knowledge, except for the studies of Boeche et al. (2011) and ours, there are no other attempts to construct a three-dimensional dependence for stars in a wide range of T_{eff} and $\log g$ (Boeche et

al., 2011; Larsen et al., 2012; Malavolta et al., 2014; Marino et al., 2008; McWilliam and Bernstein, 2008; Nissen, 1981 and references in this papers.)

To obtain a sustainable solution, we set the following boundary conditions: $\xi_{\text{turb}} = 0.55 \text{ km s}^{-1}$ for $T_{\text{eff}} = 4000 \text{ K}$, $\log g = 5.0$ and $\xi_{\text{turb}} = 7.0 \text{ km s}^{-1}$ for $T_{\text{eff}} = 10000 \text{ K}$, $\log g = 0.5 - 1.0$ (Galazutdinov et al. 2017) by adding artificial points with the appropriate values T_{eff} , $\log g$ and ξ_{turb} and specially selected weights. The set of observed values was approximated by a two-dimensional polynomial where the coefficients for all degrees of the components with respect to T_{eff} and $\log g$ (including the cross components) were calculated using the least squares method. The global minimum of the sum of the squared deviations of the weighted observed ξ_{turb} and approximated ξ_{poly} values of the microturbulence velocity was found by differentiating it with respect to all coefficients of the polynomial function and forming for them a connected coherent system of linear equations

$$\frac{d(w(\xi_{\text{turb}} - \xi_{\text{poly}})^2)}{d(a_{ij})} = 0 \quad i, j = 0 - 3, \quad (2)$$

where w —weight, ξ_{turb} —microturbulence velocity from the literature, ξ_{poly} —microturbulence velocity defined by the polynomial fit, a_{ij} —coefficients of the polynomial (see Table 1). In the process of approximation, iterative rejection of the observed values deviating from the polynomial function by more than 3σ of the current dispersion was carried out. In addition, each point was

assigned a weight w equal to $\frac{1}{\sqrt{n_{\text{loc}}}}$, where n_{loc} was determined by the number of points in sectors with $\Delta T_{\text{eff}} = 500 \text{ K}$ and $\Delta \log g = 0.5$. As a result, a uniform smooth distribution of ξ_{turb} was obtained for the 607 stars for the ranges $T_{\text{eff}} = 4000\text{--}10000 \text{ K}$ and $\log g = 0.5\text{--}5.0$ with a standard error of 0.27 km s^{-1} and the absence of dependence of this error on the atmospheric parameters.

The location of 637 sample stars on the plane $T_{\text{eff}}\text{--}\log g$ is shown in Fig. 1a with the intervals ξ_{turb} where the objects lie. Fig. 1b shows the distribution on the plane $T_{\text{eff}}\text{--}\log g$ of the sample stars ($N = 607$) used to construct the functional dependence (1) with the deviation intervals of the calculated ξ_{turb} values from the corresponding literature observational values: $\Delta \xi_{\text{turb}} = \xi_{\text{turb}}^{\text{our}} - \xi_{\text{turb}}^{\text{obs}}$. We have taken into account a relatively small number of cold $T_{\text{eff}} < 5500 \text{ K}$ MS stars. However, the available variations of ξ_{turb} in the atmospheres of such stars (no more than $\Delta \xi_{\text{turb}} = 0.3 \text{ km s}^{-1}$) and the presence of a rigidly fixed value at $T_{\text{eff}} = 4000 \text{ K}$, $\log g = 5.0$ allows one to calculate the microturbulence velocity with an average error of less than 0.27 km s^{-1} . In particular, for the solar atmosphere, the built function predicts the value $\xi_{\text{turb}} = 1.12 \text{ km s}^{-1}$, which is 0.22 km s^{-1} more than the generally accepted value. The maximum density of the points we take into account is observed in the region of MS stars with $5500 \text{ K} < T_{\text{eff}} < 7000 \text{ K}$, red subgiants and giants, which provides an average approximation

Table 1. Coefficients of the third-degree polynomial function (1).

	a_{i0}	a_{i1}	a_{i2}	a_{i3}
a_{0j}	0.943161	0.296562	$2.47216\text{E} - 2$	$-1.69846\text{E} - 3$
a_{1j}	-0.154776	-0.128602	$1.38775\text{E} - 2$	$-5.05178\text{E} - 4$
a_{2j}	0.106128	$-3.58510\text{E} - 2$	$4.91499\text{E} - 3$	$-1.43992\text{E} - 4$
a_{3j}	$-9.99955\text{E} - 3$	$5.57946\text{E} - 3$	$-9.46429\text{E} - 4$	$3.54326\text{E} - 5$

error for them of about 0.22 km s^{-1} . The density of the points is much lower in the regions of stars with higher temperatures and luminosities, and the observed ξ_{turb} values in them often vary up to $\Delta\xi_{\text{turb}} = 0.8 \text{ km s}^{-1}$ even at close atmospheric parameters. Therefore, the standard deviation of the calculated ξ_{turb} from the corresponding observed values in these regions exceeds 0.3 km s^{-1} . The largest deviation amplitude of $\Delta\xi_{\text{turb}} = 0.39 \text{ km s}^{-1}$ is observed in the MS region with temperatures of $6900 < T_{\text{eff}} < 7600 \text{ K}$ and may be due to the inclusion of several Am-stars with low turbulence velocities. In general, we can conclude that the obtained distribution allows us to determine the best ξ_{turb} values for groups of stars that make the main contribution to integrated spectra of globular clusters (F and G dwarfs of the MS, subgiants, and red giants).

Figure 2a shows in contours the distribution of ξ_{turb} values obtained using the function 1 (see also Table 1) for the entire range of parameters T_{eff} and $\log g$. It is characterized by the presence of the expected systematic increase in the micro-turbulence velocity with the increase in the effective temperature and luminosity of stars. The low degree approximating polynomial allowed us

to exclude small-scale fluctuations of the ξ_{turb} values observed in Fig. 1 in the region of hot stars that are probably due to methodological differences in determination of ξ_{turb} in different works.

Figure 2b shows in contours the distribution of ξ_{turb} values on the plane $T_{\text{eff}} - \log g$ according to the function from the paper by Boeche and Grebel (2016). Figure 2c shows the difference between our distribution of ξ_{turb} values and that obtained in Boeche and Grebel (2016).

The distribution of ξ_{turb} values in the Boeche and Grebel (2016) sample has the following important differences from our distribution: 1) the stars are mostly concentrated on the MS within the temperature range $5000 < T_{\text{eff}} < 6500 \text{ K}$ and on the sub-giant and red giant branches with $1.5 < \log g < 3.5$; 2) there are ten stars with the temperatures $6500 < T_{\text{eff}} < 7000 \text{ K}$; 3) the region of F-giants and super giants contains 20 objects with the parameters in the range $5600 < T_{\text{eff}} < 6600 \text{ K}$, $1.0 < \log g < 2.6$; 4) there are no data between the indicated areas, as well as for the temperatures higher than $T_{\text{eff}} = 7000 \text{ K}$.

Note that the function built in Boeche and

Grebel (2016) yields an increase in microturbulence velocity with increasing temperature and luminosity of stars, close to that found in our work. Our function and that of Boeche and Grebel (2016) yield the best agreement in the area of the highest data density in Boeche and Grebel (2016): on the cold side of the MS and on the branches of red subgiants and giants where the differences in the ξ_{turb} values do not exceed 0.3 km s^{-1} . Note that in these areas our function yields on average lower (by $0.05\text{--}0.15 \text{ km s}^{-1}$) microturbulence velocity values than the function of Boeche and Grebel (2016). Outside this region, the differences between the two distributions rapidly increase to 0.4 km s^{-1} for the brightest red giants, up to 0.5 km s^{-1} for MS stars with temperatures $T_{\text{eff}} > 7000 \text{ K}$, and up to 1.9 km s^{-1} for F supergiants. These differences are due to the limited set of ξ_{turb} values in Boeche and Grebel (2016), which are either small in number or completely absent in these areas. For MS stars with temperatures $T_{\text{eff}} < 5000 \text{ K}$, the function by Boeche and Grebel (2016) can yield ξ_{turb} values that are negative or close to zero due to the absence of a fixed boundary value. As a result, we can conclude that our functional dependence of the microturbulence velocity on atmospheric parameters provides correct estimates of ξ_{turb} in wide ranges of T_{eff} and $\log g$. In the areas of F- and G-dwarfs, red subgiants and giants, the results of applying our and Boeche and Grebel (2016) functions correspond to each other within the errors of these functions calculation.

Our function (1) (see also Table 1) is integrated into the program for the computing of integrated-light spectra of clusters. If any of the parameters go out of the range, we consider ξ_{turb} to be equal in its value to the nearest boundary point. Modeling the spectra of globular clusters NGC 6254 and NGC 6341 using the developed ξ_{turb} distribution leads to the average values of the microturbulence velocities: $\xi_{\text{turb}} = 1.86 \text{ km s}^{-1}$ and $\xi_{\text{turb}} = 1.88 \text{ km s}^{-1}$, correspondingly. These values are consistent within 0.20 km s^{-1} with the corresponding data found for NGC 6254 and NGC 6341 in our previous works (Khamidullina et al., 2014; Sharina et al., 2018, 2017).

4. RESULTS

4.1. Results of age, Y , $[Fe/H]$ and chemical abundances determination for Galactic globular clusters.

Table 2 lists literature data for the objects of our study obtained using their CMDs: metallicity, age, Y , color-excess and apparent distance modulus, not corrected for the Galactic extinction. The same table contains the determined in this work color-excess values and the distance modulus corrected for the Galactic extinction. These data were obtained by fitting the Bertelli et al. (2008) isochrones selected by studying the integrated-light spectra of clusters and the distribution of stars on the CMDs. The last col-

Table 2. Properties of Galactic globular clusters estimated using the analysis of stellar photometry results in this paper and in the literature: (2) metallicity from the work of Harris (1996) (H); (3) metallicity from the paper of VandenBerg et al.(2013) (V); (4)–(7) age, helium mass fraction Y , apparent distance modulus, Galactic extinction (color-excess) according to VandenBerg et al.(2013) (or in the absence of them —from the articles of Harris (1996) (H), Kruijssen et al. (2019) (K) and Testa et al. 2001 (T)). In the last three columns, our results are presented: distance modulus corrected for the Galactic extinction, color-excess and the parameters of the evolutionary isochrones (Bertelli et al., 2008) used for the spectra modeling: metallicity Z , helium mass fraction Y and logarithm of the age in Gyr. If the cluster spectrum can be adequately described using two isochrones, the index “CMD” indicates the isochrone that better describes the CMD of the cluster

Parameter/ Object	[Fe/H] ^H (dex)	[Fe/H] ^V (dex)	T ^V (Gyr)	Y ^V	(m−M) ^V (mag)	E(B−V) ^V (mag)	(m−M) ₀ ^{our} (mag)	E(B−V) ^{our} (mag)	Isochrone
(1)	(2)	(3)	(4)	(5)	(6)	(7)	(8)	(9)	(10)
NGC 1851	-1.22	-1.18	11.00	0.25	15.43	0.034	15.25	0.04	0.001,0.26,10.10
NGC 2298	-1.85	–	12.84 ^K	–	–	–	14.9	0.23	0.0004,0.26,10.05
NGC 2808	-1.15	-1.18	11.00	0.25	15.53	0.227	14.6	0.2	0.0004,0.30,10.15
	-1.15	-1.18	11.00	0.25	15.53	0.227	14.85	0.21	0.001,0.30,10.15 ^{CMD}
NGC 3201	-1.58	-1.51	11.50	0.25	14.10	0.280	13.3	0.26	0.0004,0.30,10.10
NGC 5946	-1.38	–	11.39 ^K	–	–	–	14.8 -14.9	0.13	0.0004,0.26,10.15
NGC 5986	-1.58	-1.63	12.50	0.25	–	–	15.45 - 15.4	0.305	0.0001,0.30,10.05
NGC 6171	-1.04	-1.03	12.00	0.25	14.82	0.435	14.03	0.42	0.001,0.26,10.0
NGC 6218	-1.48	-1.33	13.00	0.25	14.05	0.225	13.75	0.205	0.0004,0.26,10.10
	-1.48	-1.33	13.00	0.25	14.05	0.225	13.55	0.18	0.001,0.26,10.15 ^{CMD}
NGC 6235	-1.40	–	11.39 ^K	–	16.41 ^H	0.360 ^H	15.20	0.38	0.001,0.30,10.10 ^{CMD}
	-1.40	–	11.39 ^K	–	16.41 ^H	0.360 ^H	15.20	0.33	0.0004,0.26,10.15 ^{CMD}
NGC 6266	-1.29	–	11.78 ^K	–	15.64 ^H	0.470 ^H	14.07	0.09	0.0004,0.30,10.15
NGC 6284	-1.32	–	11.14 ^K	–	16.80 ^H	0.280 ^H	15.80	0.37	0.0004,0.30,10.10
NGC 6333	-1.75	–	–	–	15.66 ^H	0.380 ^H	–	–	0.0004,0.26,10.10
NGC 6342	-0.65	–	12.03 ^K	–	16.10 ^H	0.460 ^H	14.90	0.55	0.002,0.30,10.0
NGC 6362	-0.95	-1.07	12.50	0.25	14.58	0.076	14.46	0.08	0.001,0.30,10.15
NGC 6441	-0.53	–	11.26 ^K	–	16.79 ^H	0.470 ^H	16.0	0.49	0.001,0.26,10.0 ^{CMD}
	-0.53	–	11.26 ^K	–	16.79 ^H	0.470 ^H	15.7	0.49	0.001,0.30,10.15
NGC 6522	-1.44	–	–	–	15.94 ^H	0.480 ^H	14.57	0.10	0.0004,0.30,10.10 ^{CMD}
	-1.44	–	–	–	15.94 ^H	0.480 ^H	14.57	0.03	0.001,0.26,10.10
NGC 6544	-1.56	–	10.37 ^K	–	14.43 ^H	0.730 ^H	11.90	0.17	0.0001,0.30,10.15
NGC 6569	-0.86	–	–	–	16.85 ^H	0.550 ^H	15.10	0.06	0.001,0.23,10.15
	-0.86	–	–	–	16.85 ^H	0.550 ^H	15.25	0.06	0.001,0.26,10.05 ^{CMD}
NGC 6624	-0.42	-0.42	11.25	0.25	15.28	0.268	14.70	0.30	0.001,0.23,10.15
NGC 6626	-1.45	–	13-14	0.23 ^T	14.97 ^H	0.400 ^H	13.87	0.38	0.001,0.30,10.10
NGC 6637	-0.70	-0.59	11.00	0.25	15.23	0.163	14.80	0.18	0.002,0.23,10.10
NGC 6638	-0.99	–	–	–	16.15 ^H	0.400 ^H	14.7	0.07	0.001,0.30,10.15
NGC 6652	-0.96	-0.76	11.25	0.25	15.30 ^H	0.090 ^H	14.85	0.13	0.002,0.26,10.15
NGC 6723	-1.12	-1.1	12.50	0.25	14.73	0.070	14.65	0.09	0.001,0.26,10.10
NGC 6205	-1.54	-1.58	12.00	0.25-0.33	14.45	0.017	14.6	0.04	0.0004,0.30,10.0
NGC 7006	-1.63	–	12.25 ^K	–	18.24 ^H	0.050 ^H	17.94	0.09	0.0004,0.26,10.15

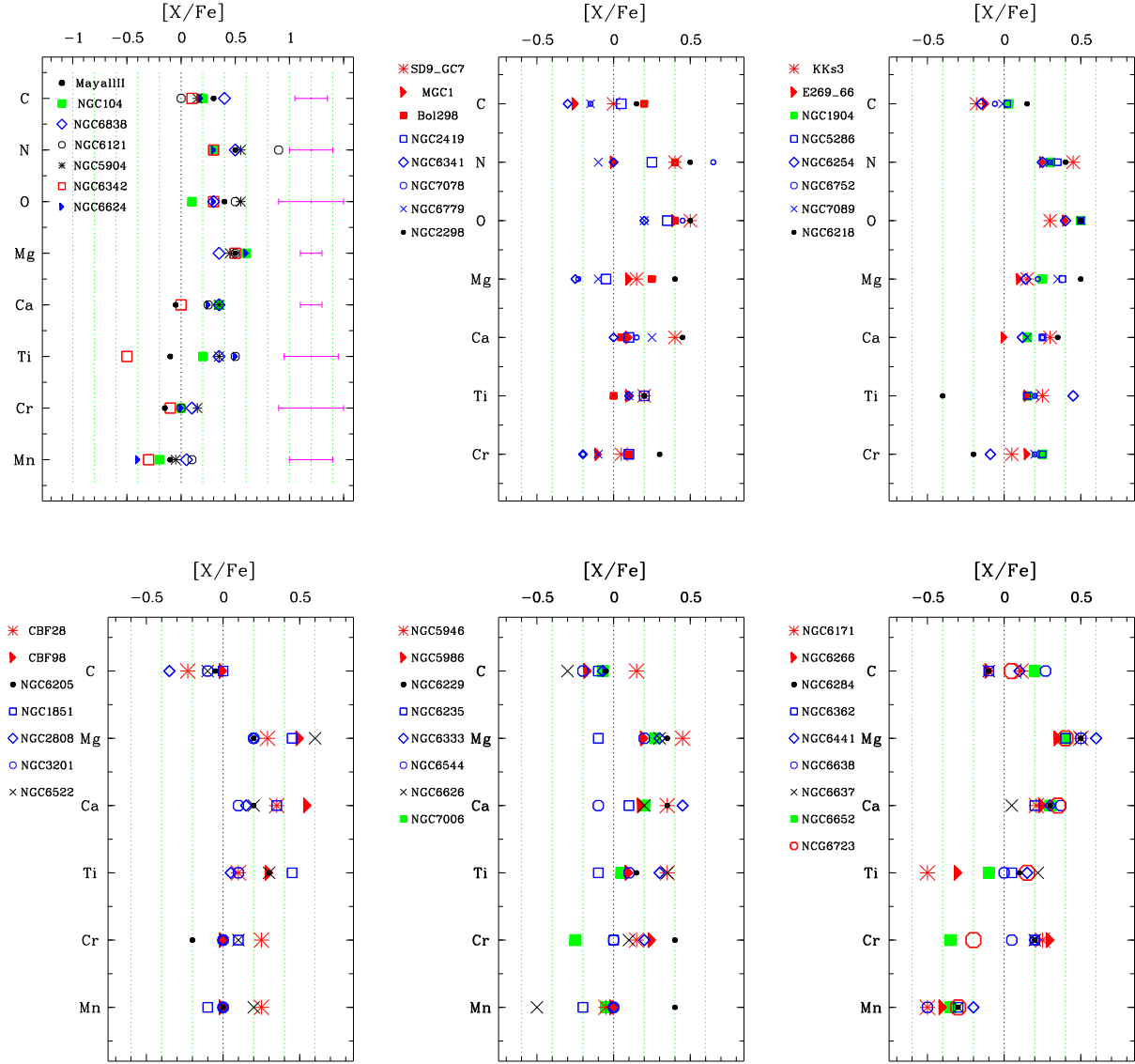


Figure 3. Chemical abundances determined using our method based on the determined evolutionary parameters (Table 3). The objects are grouped according to $[Fe/H]$. Typical abundance errors are shown in the panel (a).

umn of the table shows the parameters of the isochrones (Bertelli et al., 2008) used in modeling the spectra of clusters.

The ages, helium mass fractions (Y), metallicities ($[Fe/H]$) and abundances of chemical elements C, O, Na, Mg, Ca, Ti, Cr and Mn determined using the integrated-light spectra

analysis for the test sample of Galactic clusters are presented in Table 3 and in Figs. 3, 4 and 5. Typical errors in the determination of the listed parameters using our method and the integrated-light spectra with the signal-to-noise ratio $S/N \sim 100$ and the absence of the contribution from Galactic field stars are the fol-

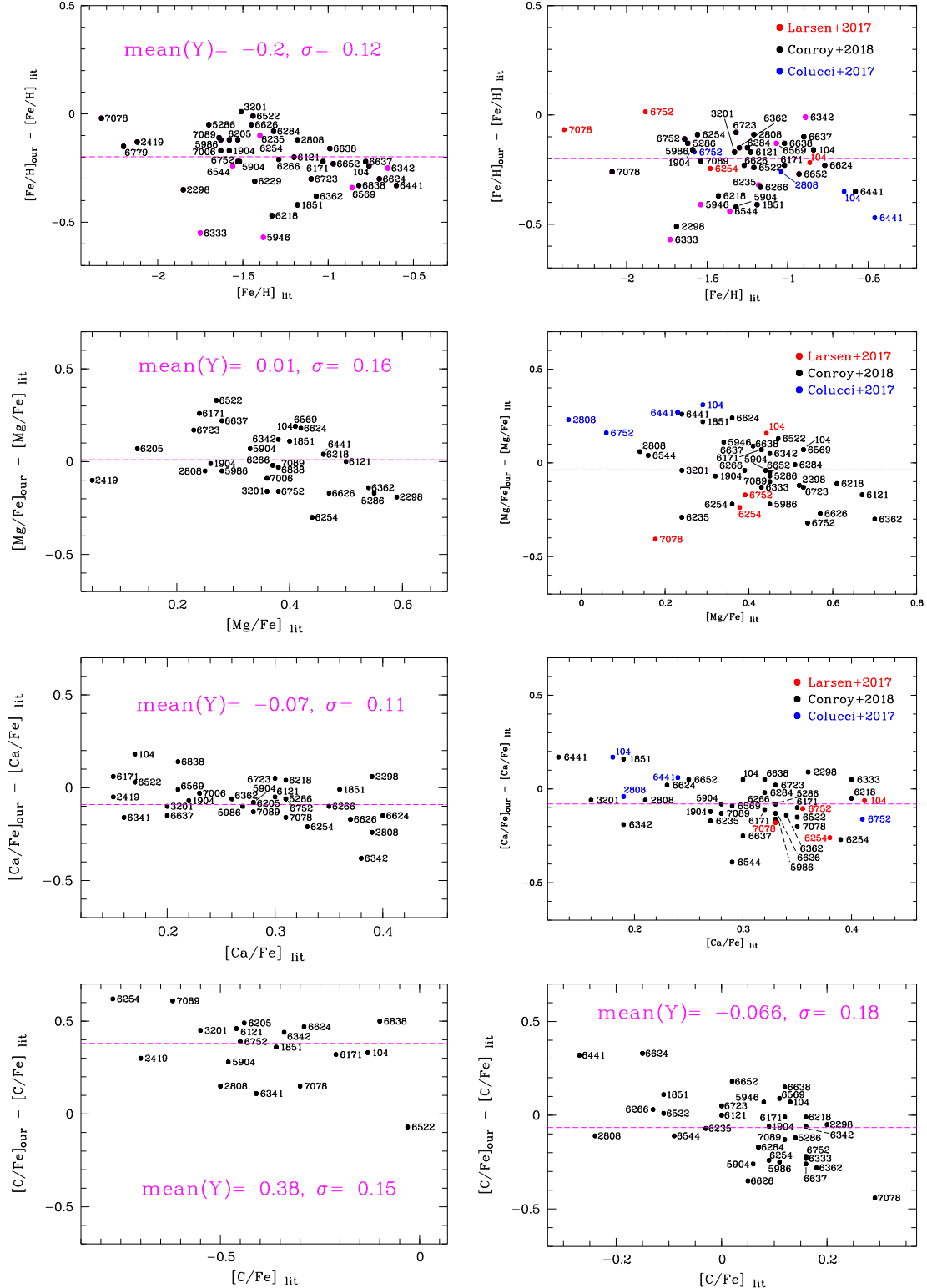


Figure 4. Comparison of the chemical abundances determined by us for Galactic GCs with the high-resolution spectroscopy results from the literature (see references in the text) (left panels) and with the literature results obtained using integrated-light spectra of the clusters (right panels). The objects with low S/N in their spectra are shown as magenta dots. NGC-numbers of the clusters are indicated.

Table 3. Age in Gyr, Y , metallicity and abundances of chemical elements determined in this study for Galactic globular clusters as a result of modeling of their integrated-light spectra. Superscript ^b denotes the clusters belonging to the bulge according to Bica et al. (2016). We obtained two complete sets of parameters for NGC 5986 and NGC 6441. For NGC 5946, NGC 6235, NGC 6522, NGC 6569, the computation with two isochrones yields similar results within the abundance measurement errors (see Table 2 and the text)

Parameter/ Object	$T_{\text{sp}}^{\text{our}}$ (Gyr)	$Y_{\text{sp}}^{\text{our}}$	[Fe/H] (dex)	[C/Fe] (dex)	[O/Fe] (dex)	[Na/Fe] (dex)	[Mg/Fe] (dex)	[Ca/Fe] (dex)	[Ti/Fe] (dex)	[Cr/Fe] (dex)	[Mn/Fe] (dex)
NGC 1851	12.6	0.26	-1.60	0.00	0.40	0.35	0.51	0.35	0.45	0.10	-0.10
NGC 2298	11.2	0.26	-2.20	0.15	0.50	0.40	0.40	0.45	0.20	0.30	0.20
NGC 2808	13.6	0.30	-1.30	-0.35	0.10	0.45	0.20	0.15	0.05	0.00	0.00
NGC 3201	12.6	0.30	-1.50	-0.10	0.30	0.20	0.20	0.10	0.10	0.00	0.00
NGC 5946	12.6,13.6	0.26	-1.95	0.15	0.55	0.45	0.45	0.35	0.35	0.15	-0.05
NGC 5986	12.5	0.30	-1.75	-0.10	0.30	0.00	0.25	0.15	0.10	0.20	0.20
	11.2	0.30	-1.75	-0.17	0.30	0.00	0.20	0.18	0.10	0.25	0.00
NGC 6171	10.0	0.26	-1.25	0.11	0.30	0.20	0.50	0.21	-0.50	0.25	-0.50
NGC 6218	12.6,13.6	0.26	-1.80	0.15	0.50	-0.10	0.50	0.35	-0.40	-0.20	-0.50
NGC 6235	12.6,13.6	0.26,0.30	-1.50	-0.10	0.30	0.20	-0.05	0.10	-0.10	0.00	-0.20
NGC 6266	13.6	0.30	-1.50	-0.10	0.30	0.20	0.35	0.25	-0.30	0.30	-0.40
NGC 6284	12.6	0.30	-1.40	-0.10	0.30	0.50	0.50	0.30	0.10	0.20	-0.30
NGC 6333	12.6	0.26	-2.30	-0.07	0.30	0.20	0.30	0.45	0.30	0.20	0.00
NGC 6342 ^b	12.6	0.23	-0.90	0.10	0.30	0.20	0.50	0.00	-0.50	-0.10	-0.30
NGC 6362 ^b	13.6	0.30	-1.45	-0.10	0.30	0.50	0.40	0.20	0.05	0.20	-0.30
NGC 6441	10.0	0.26	-0.90	0.10	0.35	0.40	0.60	0.30	0.15	0.20	-0.20
	13.6	0.30	-0.95	0.00	0.30	0.20	0.40	0.30	0.10	0.00	0.00
NGC 6522 ^b	12.6	0.30,0.26	-1.45	-0.10	0.30	0.20	0.60	0.20	0.30	0.10	0.2
NGC 6544	13.6	0.30	-1.80	-0.20	0.30	0.20	0.20	-0.10	0.10	0.00	0.00
NGC 6569	13.6,11.2	0.23,0.26	-1.20	0.20	0.30	0.40	0.60	0.20	0.40	0.20	0.00
NGC 6624 ^b	13.6	0.23	-1.00	0.18	0.30	0.40	0.60	0.25	0.50	0.00	-0.40
NGC 6626 ^b	12.6	0.30	-1.50	-0.30	0.30	0.45	0.30	0.20	0.35	0.10	-0.50
NGC 6637 ^b	12.6	0.23	-1.00	-0.10	0.30	0.10	0.50	0.05	0.22	0.20	-0.30
NGC 6638	13.6	0.30	-1.15	0.27	0.30	0.20	0.50	0.37	0.00	0.05	-0.50
NGC 6652	13.6	0.26	-1.20	0.20	0.30	0.45	0.40	0.3	-0.10	-0.35	-0.35
NGC 6723 ^b	12.6	0.26	-1.40	0.05	0.30	0.50	0.40	0.35	0.15	-0.20	-0.30
NGC 6205	10.0	0.30	-1.70	-0.12	0.3	0.70	0.20	0.20	0.30	-0.20	0.00
NGC 7006	13.6	0.26	-1.8	-0.07	0.45	0.40	0.27	0.20	0.05	-0.25	-0.05

lowing: $\sigma[\text{C/Fe}] \sim 0.2$ dex, $\sigma[\text{O/Fe}] = 0.3$ dex, and Y determination approximately corresponds $\sigma[\text{Na/Fe}] \sim 0.2$ dex, $\sigma[\text{Mg/Fe}] \sim 0.15$ dex, to half the step of the stellar evolution models $\sigma[\text{Ca/Fe}] \sim 0.1$ dex, $\sigma[\text{Ti/Fe}] \sim 0.2$ dex, used in these parameters (see Khamidullina et al., 2014; Sharina et al. 2014, 2013, 2018, 2017). $\sigma[\text{Cr/Fe}] \sim 0.2$ dex and $\sigma[\text{Mn/Fe}] \sim 0.2$ dex, $\sigma[\text{Fe/H}] \sim 0.1$ dex. The accuracy of the age It should be noted that the oxygen lines are too

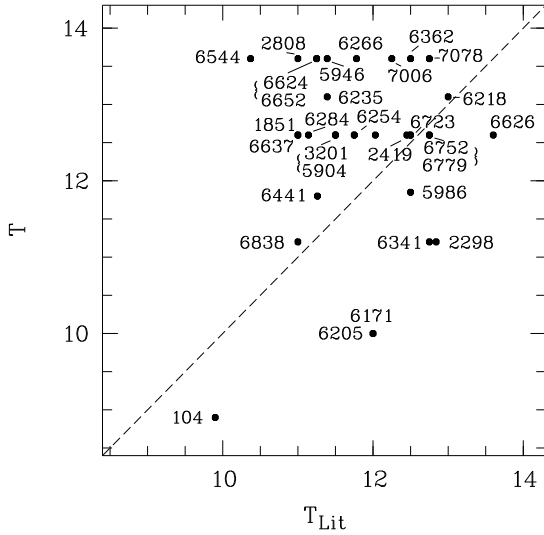


Figure 5. Comparison of the age estimates determined from the analysis of their integrated-light spectra for Galactic globular clusters with the values obtained in the literature using CMDs of the clusters for all objects except NGC 104 (see Sec. 4.3).

weak and not visible in the spectrum for the spectral range and resolution that we use. However, the oxygen abundance affects the formation of the molecular balance of CN and CH due to the partial binding of carbon to the CO molecule. We usually set $[O/Fe] = 0.3$ when started modeling the spectra. In some cases, this content had to be slightly changed (Table 3) so that the profiles of the molecular bands CN and CH were reproduced correctly. The intensities of these bands are influenced by the lines of C, N, O and other elements.

In Figs. 4 and 5, we present a comparison of the chemical abundances and ages determined for the clusters with the corresponding literature values. We selected literature $[Fe/H]$ values mainly from the papers by VandenBerg et al. (2013)

and Harris (1996). For NGC 6624, NGC 6341, NGC 6637 and NGC 6652 $[Fe/H]$, the values were taken from Forbes and Bridges (2010), and for NGC 6779,- from Dotter et al. (2010). Literature abundances of chemical elements were taken mainly from Pritzl et al. (2005) and Roediger et al. (2014). We found the missing data on the abundances in the following papers: Johnson et al. (2017) for NGC 5986; Mészáros et al. (2015) for NGC 6171 and NGC 6205; Yong et al. (2014) for NGC 6266 and Massari et al. (2017) for NGC 6362.

4.2. Comparison of the observed and synthetic integrated-light spectra

The SAO ftp site² contains the figures of the comparison of the observed spectra of 26 Galactic globular clusters from the paper by Schiavon et al. (2005) and the spectroscopic OHP archive with the synthetic spectra calculated using models of stellar atmospheres. Also, it includes a comparison of literature stellar photometry results in these globular clusters (Sarajedini et al., 2007; Piotto et al., 2002) with the stellar evolutionary isochrones selected based on the best description of the hydrogen lines in the observed spectra. Here, we present the aforementioned comparison for only one object. Figure 6 (top panel) shows the comparison of the stellar photometry results (Sarajedini et al., 2007)

² <ftp://ftp.sao.ru/pub/sme/AnalILMWGCs/>

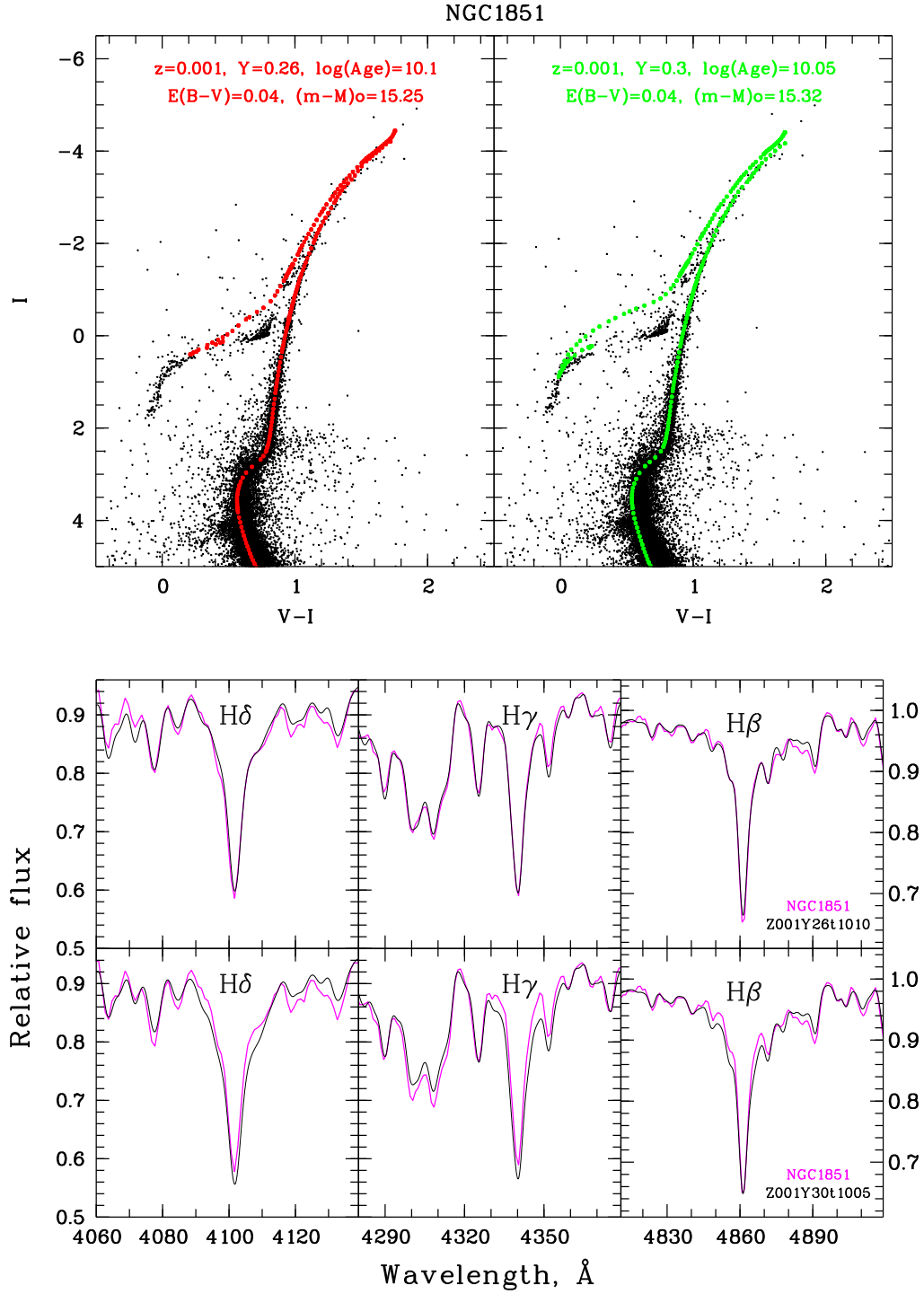


Figure 6. Comparison of the stellar photometry results for the Galactic globular cluster NGC1851 (Sarajedini et al., 2007) with the theoretical stellar evolutionary isochrones (Bertelli et al., 2008) (top panel). Comparison of the hydrogen lines in the observed spectrum of NGC1851 (Schiavon et al., 2005) with the synthetic ones (black) representing the integrated light of the cluster and computed using the isochrones demonstrated in the top panel (bottom panel).

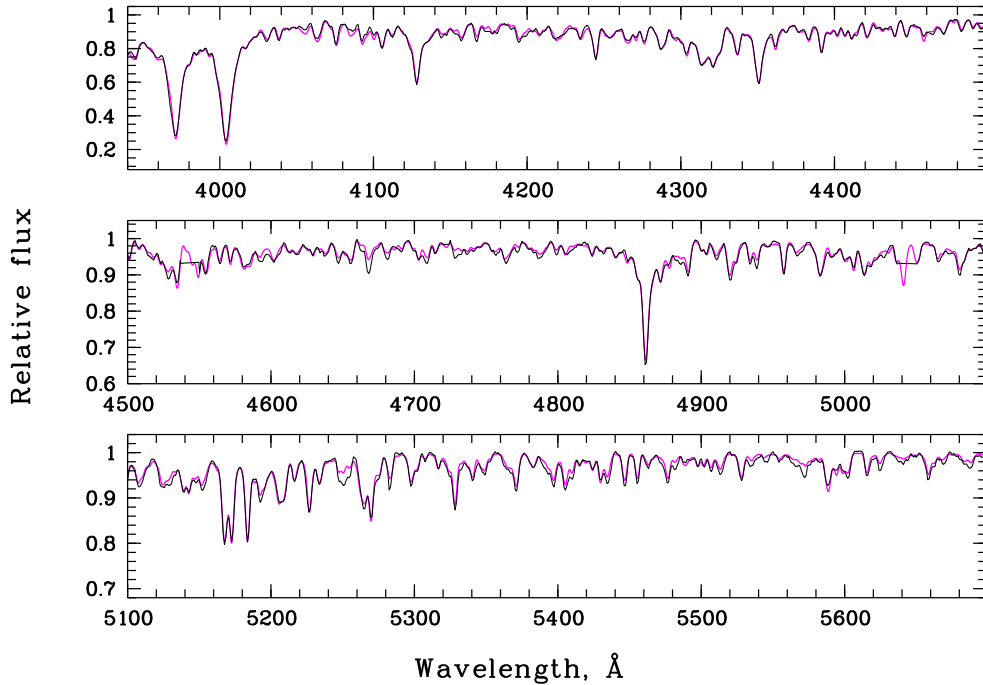


Figure 7. Comparison of the spectrum of NGC 1851 (black) (Schiavon et al., 2005) with the synthetic spectrum of the cluster (see text).

with two isochrones (Bertelli et al., 2008) selected based on the best fitting of the hydrogen lines by the model ones. Both isochrones describe the distribution of stars on the CMD correctly, except for the HB stage. The horizontal branch is not described precisely in either case. The comparison of the hydrogen line profiles in the observed and synthetic spectra calculated using two isochrones shows that an isochrone with the absence of the extremely blue HB stars is more suitable: $Z = 0.001$, $Y = 0.26$, $\log T = 10.10$. It can be assumed that the integrated spectrum of the cluster contains a relatively small number of such objects. Figure 7 shows a complete comparison of the observed and synthetic spectra. The model spectrum

was computed using the isochrone $Z = 0.001$, $Y = 0.26$, $\log T = 10.10$ and abundances from Table 3. Note, that the spectra of globular clusters NGC 5946, NGC 6235, NGC 6333, NGC 6342, NGC 6544, NGC 6569 from Schiavon et al. (2005) have rather low S/N . This can be seen in the figures of their comparison with the model spectra presented on the SAO ftp site.

Figure 3 shows the estimates of the abundances derived by us together with the data from our previous works for the Galactic (NGC 104, NGC 1904, NGC 2419, NGC 2808, NGC 3201, NGC 5286, NGC 5904, NGC 6121, NGC 6205, NGC 6254, NGC 6341, NGC 6752, NGC 6779, NGC 6838, NGC 7089) and extragalactic (Mayall II, SD9-

GC7, MGC1, Bol298, GC-KKs3, GC-E269-66, CBF28, CBF98) clusters: Khamidullina et al. (2014); Sharina et al. (2014); Sharina and Shimansky (2020); Sharina et al. (2013, 2018, 2017). The objects are grouped according to their $[\text{Fe}/\text{H}]$ values. Typical errors of the abundances are shown in the top left panel. This panel summarizes the data for the objects with $[\text{Fe}/\text{H}] \sim -1$ dex. The middle top panel of Fig. 3 shows abundances of chemical elements for the clusters with $[\text{Fe}/\text{H}] \sim -2$ dex. Other panels of the figure demonstrate the objects with $[\text{Fe}/\text{H}] = -1.5 \pm 0.25$ dex.

4.3. Comparison of our and literature age estimates

Comparison of our and literature data was carried out for the full sample of 40 clusters, which is described in Section 2. We used the available literature estimates by VandenBerg et al. (2013) and the absent values were taken from the papers by Kruijssen et al. (2019) and Testa et al. (2001). We used the age 9.9 ± 0.7 Gyr for NGC104 determined by Hansen et al. (2013) during the investigation of its white dwarf sequence. It should be noted that literature data about the absolute age of NGC104 are quite different (Brogaard et al., 2017). When comparing our and literature estimates of age, we considered all literature age values greater than the age of the Universe to be equal to 13.6 billion years. We did not manage to find in the literature absolute

age values for five sample clusters: NGC6229, NGC6333, NGC6522, NGC6569, NGC6638. A comparison of our absolute age estimates with the corresponding literature values (Fig. 5) shows that the moduli of the differences between them are more than 1.4 billion years for 14 objects, that is, for 40% of the sample. Let us briefly consider the reasons of these deviations and, in general, the reasons behind the significant differences in the estimates of the absolute ages of Galactic globular clusters by different authors.

More than half of the 14 objects are located close to the plane of the Galaxy and have a significant color excess $E(B - V) \geq 0.3$ (Harris, 1996; Schlegel et al., 1998). In such cases, the quality of the spectrum is determined not only by the brightness of the object itself but also by the influence of a large number of background stars. They contribute both to the total spectrum of the cluster and to the total spectrum of background stars, which is subtracted from the spectrum of the cluster. Thus, due to significant inhomogeneities in the field, the influence on the spectrum of the field stars can be overestimated or underestimated. The intensities and shapes of the lines of hydrogen and of various chemical elements in the integrated-light spectra may be randomly distorted. Therefore, we meet inevitable difficulties in the analysis of the spectra. Moreover, Schiavon et al. (2005) noted that the spectra of clusters at low galactic latitudes can be distorted by weak emission lines of the galactic background. Note that the described difficulties

in obtaining and analyzing integrated-light spectra are significant for the objects of our Galaxy, which are large in projection onto the celestial sphere, that is, the probability of the field pollution of their spectra is high.

Furthermore, for nine of the aforementioned 14 objects, the metallicity is $[\text{Fe}/\text{H}] \leq -1.4$ dex. It has long been established that the well-known age-metallicity degeneracy problem is more difficult to solve for low metallicities (see e.g. VandenBerg et al. (2013), Pietrinferni et al. (2013)). This is mainly due to the negligible changes in the observed parameters that occur in this case with varying the metallicities. In addition, let us note that the results of age and metallicity determination using color-magnitude diagrams depend on the adopted oxygen abundance in stellar population models (Denissenkov et al., 2017; VandenBerg et al., 2013). The situation is complicated by Na-O anticorrelations in globular clusters.

For seven objects in the sample, the absolute values of the differences between the literature and our age estimates exceed 2 Gyr:

NGC 2808: $|\Delta(T)| = 2.6$ Gyr, $E(B-V) = 0.23$ mag,
 NGC 5946: $|\Delta(T)| = 2.2$ Gyr, $E(B-V) = 0.54$ mag,
 NGC 6171: $|\Delta(T)| = 2.0$ Gyr, $E(B-V) = 0.33$ mag,
 NGC 6205: $|\Delta(T)| = 2.0$ Gyr, $E(B-V) = 0.02$ mag,
 NGC 6544: $|\Delta(T)| = 3.23$ Gyr, $E(B-V) = 0.73$ mag,
 NGC 6624: $|\Delta(T)| = 2.35$ Gyr, $E(B-V) = 0.28$ mag,
 NGC 6652: $|\Delta(T)| = 2.35$ Gyr, $E(B-V) = 0.09$ mag.

As it was mentioned in Section 4.2, NGC 5946 and NGC 6544 have low S/N ratio in their spectra. Color excess values $E(B-V)$ for all objects, except NGC 2808, NGC 6205 and NGC 6652, are greater or equal to 0.3 (Harris 1996; Schlegel et al., 1998). Probably, the spectra of these objects were contributed by background stars.

Let us analyze the reasons for the discrepancy between our and literature age data for three clusters with low $E(B-V) = 0.09$. NGC 2808 is an unusual cluster, whose stars show significant variations in the helium content at a constant nitrogen abundance, similar to that found in field stars (Cabrera-Ziri et al. (2019) and references therein). Significant scatter of colors and luminosities of stars relative to the inscribed evolutionary sequences can be seen on the CMD of the cluster³ plotted according to the stellar photometry results of Sarajedini et al. (2007). Our analysis of the spectrum of the cluster reveals the metallicity lower than it follows from the analysis of the object's CMD. We did not manage to describe the horizontal branch of NGC 2808 by isochrones (Bertelli et al., 2008). It is wide, extremely extended to the blue side with a large number of faint stars on the blue end and bright stars on the red end. More detailed spectroscopic studies, determination of the helium content of individual stars, and more sophisticated stellar evolution models are needed to better un-

³ ftp://ftp.sao.ru/pub/sme/AnalILMWGCs/NGC1851_2298_2808_3201.pdf

derstand the properties of the integrated light of NGC 2808.

NGC 6205 (M 13) is a nearby, bright and well-studied object. Narrow evolutionary sequences and extremely blue horizontal branch can be seen at the cluster CMD⁴ according to the stellar photometry results (Sarajedini et al., 2007). The specific helium content varies significantly among cluster stars (Denissenkov et al., 2017). These authors observed unusually high periods of the RR Lyr stars in the object. We did not manage to describe the integrated-light spectrum of NGC 6205 with the Bertelli et al. (2008) models. The spectrum of NGC 6205 we used was obtained from observations in OHP in one spectroscopic slit position during 300 sec. and is not representative of the total stellar population of the cluster. The younger age derived by us likely indicates that quite a few blue hot horizontal branch fell into the slit during observations.

In the article by Sharina et al. (2020), we analyzed the spectrum of NGC 6652 from Schiavon et al. (2005). In that study, the observed spectrum was compared with synthetic spectra calculated using not only the Bertelli et al. (2008) isochrones, but also the Teramo group isochrones (Pietrinferni et al., 2013) as well as using different stellar mass functions. There is still no consensus in the literature about the age of NGC 6652 and its association with the Galactic substructures (e.g. Sharina et al., 2020) and

references therein). Our analysis of the cluster spectrum from Schiavon et al. (2005) argues in favor of the presence of blue horizontal branch stars in NGC 6652. Our results indicate that the stellar population of the object can be characterized by the chemical composition and age typical of the Galactic bulge globular clusters. The study of the shapes and depths of the hydrogen lines in combination with the analysis of the distribution of stars on the cluster CMD has led to the conclusion that NGC 6652 is older than it was accepted in the literature: 13.6 Gyr instead of 11.7 Gyr (Chaboyer et al., 2000), or 11.25 Gyr (Van den Berg et al., 2013).

4.4. Comparison of the abundances with literature data

Figure 4 (left panels) represents the differences between the elemental abundances determined in this study and the corresponding literature values from high-resolution spectroscopic studies of the brightest cluster stars. The mean difference and the standard error of the mean are given in each panel legend. There are no significant systematic differences, except for the cases of [Fe/H] and [C/Fe]. It can be seen in Fig. 4 that [Fe/H] values determined by us are on average 0.2 dex less than the literature ones. This is a distinctive feature of our method in its current state. A possible reason may be an overestimation of the ξ_{turb} values used by us, which affect the line intensities in the synthetic spectra

⁴ ftp://ftp.sao.ru/pub/sme/AnalILMWGCs/NGC6638_6652_6723_6205_7006.pdf

and the abundances of chemical elements. The overestimation of ξ_{turb} lowers the abundances of chemical elements, primarily iron, whose lines prevail in the spectra. The question needs further investigation. The reasons for the systematic differences of $[\text{C}/\text{Fe}]$ will be discussed later in this section.

The deviations of $[\text{Fe}/\text{H}]$ values from literature values are larger than for other sample clusters for several objects with $[\text{Fe}/\text{H}]$ in the range $[-1.8; -1]$ dex. These are NGC 1851, NGC 3201, NGC 6218, NGC 6333, NGC 6362 and NGC 5946. As it was mentioned earlier in this paper, NGC 6333 and NGC 5946 have low S/N in their spectra. Let us consider the cases of NGC 1851, NGC 6218, NGC 6362 and NGC 3201 in more detail.

The deviation of the $[\text{Fe}/\text{H}]$ value for NGC 1851, and probably for many other clusters in the sample, is likely due to the fact that we use scaled solar isochrones of stellar evolution and models of stellar atmospheres. Elemental abundance ratios differ significantly from those of the Sun in NGC 1851, the globular cluster Omega Centauri and several other galactic clusters. NGC 1851 contains so called “anomalous” second generation stars (see e.g. Simpson et al., 2017) and references therein). Variations of C, N, O elemental abundances in them correlate with the abundances of s -process elements and with the metallicity $[\text{Fe}/\text{H}]$. Typically, two stellar populations exist in such “anomalous” clusters: s -element/Fe-rich and

s -element/Fe-poor. Four stellar populations were found in NGC 1851 (Simpson et al. 2017 and references therein). A more detailed investigation of the integrated-light spectrum of this cluster would be desirable.

The large deviation of $[\text{Fe}/\text{H}]$ from the literature value for NGC 6218 is apparently due to two main reasons. First, the Poisson noise in the spectrum is quite large⁵, especially in its red part, the lines in which are mainly used for metallicity determination. The cluster is located at a low Galactic latitude. Therefore, the background subtraction result may be imperfect. Second, the cluster is unusual, with an extremely blue horizontal branch. It can be seen from the figures presented on the ftp-site that the isochrones by Bertelli et al. (2008) selected for modelling the spectrum do not describe perfectly either the spectrum or the CMD of the cluster. Probably, the reason is in the significantly non-solar elemental abundance ratios for NGC 6218 (see e.g. Mishenina et al., 2003).

During the observations of NGC 6362, Schiavon et al. (2005) encountered problems with the line widths in the calibration spectrum of the arc lamp (Section 3.5.2 in Schiavon et al., 2005). Therefore, the authors advised to use this spectrum only for low-resolution analysis.

NGC 3201 has a loose structure and is located at a low Galactic latitude. Schiavon et al. (2005) discovered the emission line $[\text{O II}] \lambda 3727 \text{ \AA}$ in its

⁵ ftp://ftp.sao.ru/pub/sme/AnalILMWGCs/NGC5946_5986_6171_6218.pdf

integrated-light spectrum and suggested that the Balmer series lines can also be distorted by weak HII-emission of the galactic background. We have managed to fit the hydrogen lines in the spectrum of NGC 3201 by the model ones. However, the S/N ratio in the spectrum is quite low⁶, and this fact also influenced the fitting results.

In the following, we will continue the comparison of our and literature results. Figure 4 (right panels) demonstrates that the abundances of elements determined by us are consistent within the errors with the literature values obtained by studying the integrated spectra of the clusters. For some objects, there are systematic differences between our and literature data. For example, the estimates by Colucci et al. (2017) of $[Mg/Fe]$ abundances in four objects common with our sample are lower on average by 0.2 dex than our estimates. The estimates by Larsen et al. (2017) of $[Mg/Fe]$ abundances in NGC 7078, NGC 6254, and NGC 6752 are somewhat higher than our estimates.

The reasons for the differences may lie not only in the dissimilarities between the applied methods, but also in the contribution of various stars into the integrated spectra analyzed by the authors. The spectra were obtained using different telescopes and spectrographs. It is possible that background stars fall into the integrated spectra. Conroy et al. (2018) uses the spectra from Schiavon et al. (2005), that is, the

same data that we analyzed. The $[Mg/Fe]$ estimates made by Conroy et al. (2018) are on average consistent with our results. The variance of the differences is 0.16 dex and corresponds to the average abundance estimation error. Let us recall that some spectra of objects from Schiavon et al. (2005) were obtained with a relatively low signal-to-noise ratio. A number of clusters are close to the Galactic plane. Therefore, despite of a careful background subtraction, their spectra can be significantly changed by background stars.

Note the difference between the $[C/Fe]$ values obtained using the integrated spectra of clusters and the spectra of their brightest stars (Fig. 4, two bottom panels). While the average difference between our estimates and the Conroy et al. (2018) data is -0.066 dex, the difference between our $[C/Fe]$ for the clusters and the mean $[C/Fe]$ of the brightest stars in the clusters is on average $+0.38$ dex. We interpret the latter as the effect of a change in the chemical composition of the atmospheres of stars in the course of their evolution (Kraft, 1994).

5. ELEMENTAL ABUNDANCES IN GLOBULAR CLUSTERS DEPENDING ON METALLICITY AND COMPARISON WITH CHEMICAL EVOLUTION MODELS

The distribution of the abundances of chemical elements for 40 Galactic globular clusters

⁶ ftp://ftp.sao.ru/pub/sme/AnalILMWGCs/NGC1851_2298_2808_3201.pdf

are shown in Fig. 8. The mean abundance values and the standard deviations for 40 objects are the following: $[C/Fe] = -0.025 \pm 0.17$ dex, $[Mg/Fe] = 0.32 \pm 0.22$ dex, $[Ca/Fe] = 0.22 \pm 0.12$ dex, $[Ti/Fe] = 0.14 \pm 0.24$ dex, $[Cr/Fe] = 0.05 \pm 0.16$ dex, $[Mn/Fe] = -0.17 \pm 0.22$ dex, $[Na/Fe] = 0.3 \pm 0.2$ dex.

It can be seen in Fig.3 that, in general, in three groups of clusters with different metallicities, the distributions of the abundances look similar.

The majority of the sample objects have $[Fe/H] \leq -1.0$ dex and apparently belong to the Galactic halo divided by the internal and the external components according to Carretta et al. [10]. The problems of separation of clusters into subsystems are discussed e.g. by Marsakov et al. (2019). A part of our sample clusters belongs to the Galactic bulge (Bica et al., 2016): NGC 6342 ($[Fe/H]_{\text{our}} = -0.9$, $[Mg/Fe]_{\text{our}} = 0.5$), NGC 6522 (-1.45 , 0.6), NGC 6624 (-1.0 , 0.6), NGC 6626 (-1.5 , 0.3), NGC 6637 (-1.0 , 0.5), NGC 6723 (-1.4 , 0.4). Some of our sample objects, apparently, fell into the bulge region from the outer parts of the Galaxy (Bica et al., 2016): NGC 6333 ($[Fe/H]_{\text{our}} = -2.3$, $[Mg/Fe]_{\text{our}} = 0.3$), NGC 6171 (-1.25 , 0.5), NGC 6235 (-1.5 , -0.05), NGC 6441 (-0.9 , $[0.4; 0.6]$), NGC 6544 (-1.8 , 0.2), NGC 6569 (-1.2 , 0.6). Some metal-rich clusters of our sample are observed outside the bulge, i.e. at the distances from the Galactic center larger than 4.5 Kpc: NGC 104 ($[Fe/H] = -1.0$, $[Mg/Fe] = 0.6$, (Sharina et al., 2018), NGC 6362 ($[Fe/H]_{\text{our}} = -1.45$, $[Mg/Fe] = 0.4$). Bica et

al. (2016) concluded that the distributions of the abundances of alpha-process elements (O, Mg, Si, and Ca) depending on $[Fe/H]$ in the bulge clusters and field stars are similar.

Abundances of chemical elements provide important information about supernovae (SNe) and other stars that contributed to the formation of the chemical composition of the studied objects and subsystems of the galaxies containing them. Let us compare the estimated elemental abundances with the model ones in the theory of chemical evolution by Kobayashi et al. (2006). These authors investigated the production of elements by type II supernovae (SNe II) and hypernovae. Kobayashi et al. (2006) built chemical evolution models for the halo, bulge and thick disk of our Galaxy. These three models show significant differences in chemical abundances (in comparison with our corresponding errors of their determination) for O, Mg, Ca, Ti, Cr and Mn only in the metallicity range $[Fe/H] \leq -2.5$ and $[Fe/H] \geq 1.0$ (Fig. 32 in Kobayashi et al., 2006).

Let us consider the distribution of the model elemental abundances depending on $[Fe/H]$ presented in Kobayashi et al. (2006) for the metallicity range $-2 \leq [Fe/H] \leq -1$ dex, where the objects of our sample are mainly located. The elements O and Mg were produced mainly in the process of the hydrostatic combustion in SNe II, and their abundances depend on the supernova model. In the paper by Kobayashi et al. (2006) $[O/Fe] \sim 0.42$ at $[Fe/H] = -1.0$ dex

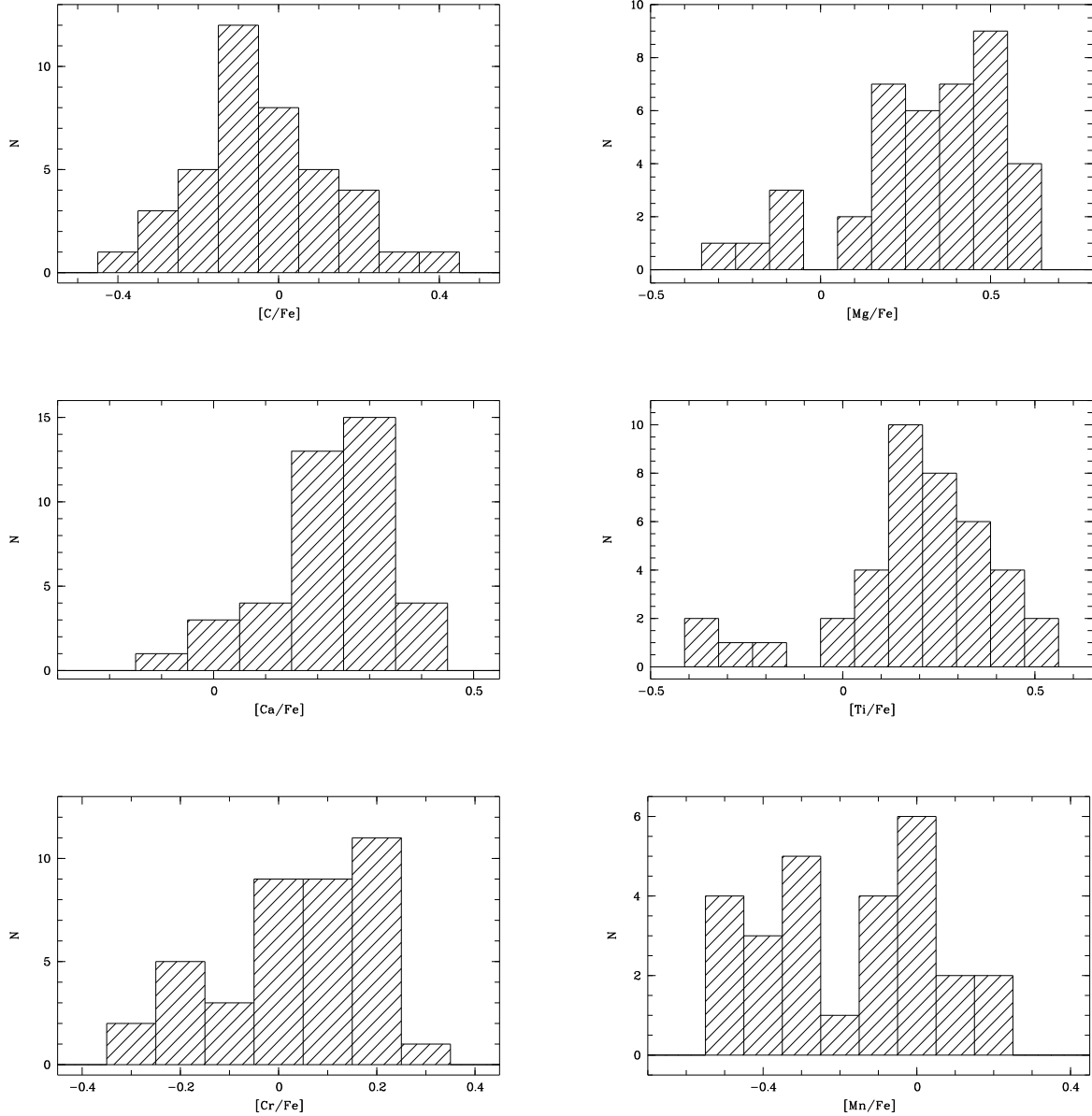


Figure 8. Distributions of the determined abundances of chemical elements for 40 Galactic globular clusters (see text).

and is approximately constant in the range $-2 \leq [\text{Fe}/\text{H}] \leq -1$. Let us recall that we set the values of $[\text{O}/\text{Fe}] \sim [0.3; 0.5]$ for the studied objects. These values are in agreement with the results of Kobayashi et al. (2006).

Model abundances of other α -process

elements are approximately constant in this metallicity range: $[\text{Mg}/\text{Fe}] \sim 0.49$ dex, $[\text{Ca}/\text{Fe}] \sim 0.27\text{--}0.39$ dex (Kobayashi et al., 2006). The observed reduced abundances $[\text{El}/\text{Fe}]$ of the alpha-process elements can be explained by SNe Ia bursts, which produce

mainly iron, and also by the bursts of low-mass SNeII (13–15 M_{\odot}) (Kobayashi et al., 2006). Our results for Mg and Ca are consistent with the model data (Fig. 8) for the majority of the studied objects. We have determined negative [Mg/Fe] values for NGC 2419, NGC 6235, NGC 6341, NGC 6779 and NGC 7078. All these clusters, except NGC 6235, have low metallicity $[\text{Fe}/\text{H}] \leq -2$ dex. NGC 2419 is the most distant massive Galactic globular cluster with significant chemical anomalies (see e.g. Sharina et al. (2013) and references therein). A negative [Ca/Fe] value was obtained by us only for NGC 6544.

The average model [Ti/Fe] abundance is -0.1 dex (Kobayashi et al., 2006). The authors note that the observed values are systematically higher than the model ones by approximately 0.4 dex. The [Ti/Fe] values determined by us are basically larger than zero. Negative values were derived for NGC 6171, NGC 6218, NGC 6235, NGC 6266, NGC 6342, NGC 6652. A part of these objects reside in the bulge: NGC 6171, NGC 6235, NGC 6342.

The main sources of carbon and nitrogen are the asymptotic branch, Wolf-Rayet, and low-mass stars with masses less than the mass of the Sun. The contribution of these sources is not included in the calculations by Kobayashi et al. (2006). Model carbon abundances vary approximately from -0.25 to -0.2 dex in the metallicity range $-2 \leq [\text{Fe}/\text{H}] \leq -1$ dex. The carbon abundances determined in this paper, as well as the observational data for field stars from the lit-

erature (Kobayashi et al., 2006) vary in a wide range (Fig. 8).

Abundances of the odd Z -elements (Na, Al and Cu) depend strongly on metallicity (Kobayashi et al., 2006). Note that, for Na, it is necessary to take into account non-LTE effects in the atmospheres of stars with $[\text{Fe}/\text{H}] \leq -2.0$ dex. Model abundances of Na increase approximately from -0.1 to 0.3 dex in the metallicity range $-2 \leq [\text{Fe}/\text{H}] \leq -1$ (Kobayashi et al., 2006). The abundances of Na were confidently determined by us not for all the sample objects, since the only way to accomplish this task was to use weak lines Na I 5682Å, 5688Å. Furthermore, the spectra from Schiavon et al. (2005) have a relatively low S/N in the red spectral range. Our estimates are within the range $-0.2 \leq [\text{Na}/\text{Fe}] \leq 0.7$ (Table 3).

Model abundances of the iron group elements Cr and Mn are approximately constant in the metallicity range $-2 \leq [\text{Fe}/\text{H}] \leq -1$: $-0.5 \leq [\text{Mn}/\text{Fe}] \leq -0.6$, $[\text{Cr}/\text{Fe}] \sim 0.1$. Spectral lines of Mn and Cr are rather weak in the used spectra. It can be seen in Fig. 8 that our estimates of the Mn and Cr abundances vary widely, and the objects with $[\text{Mn}/\text{Fe}] \geq 0$ are NGC 2298, NGC 2419, NGC 5986, NGC 6522 (Table 3).

Matteucci et al. (2019) have presented chemical evolution models for the bulge and the inner Galactic disk. The models by Matteucci et al. differ by the star-formation rate and efficiency, initial mass function [Salpeter (1955), Calamida et al. (2015), Kroupa et al. (1993)] and by the

sources of chemical evolution yields of SNe Ia. As it can be seen in figures presented by Matteucci et al.(2019), that the theoretical distribution $[\text{Mg}/\text{Fe}]$ versus $[\text{Fe}/\text{H}]$ for different models, except the model for the disk, is approximately the following: $[\text{Mg}/\text{Fe}] \sim 0.43$ at $[\text{Fe}/\text{H}] = -2.0$, then the rise up to the values $[\text{Mg}/\text{Fe}] \sim 0.5$ at $[\text{Fe}/\text{H}] = -1.3$, and then the decline to the previous value $[\text{Mg}/\text{Fe}] \sim 0.43$ at $[\text{Fe}/\text{H}] = -0.7$. Our Mg abundances for the sample clusters in the bulge and for NGC 104 and NGC 6362 are generally consistent with this model within our errors of the abundances determination (Figs. 4, 3).

6. CONCLUSION AND FURTHER PERSPECTIVES

Long-slit medium-resolution integrated-light spectra of 26 Galactic globular clusters were used to determine the age, helium mass fraction (Y), metallicity ($[\text{Fe}/\text{H}]$), and abundances of chemical elements C, O, Na, Mg, Ca, Ti, Cr and Mn. Our method, described in Section 3 was applied. It was supplemented in this paper by automatically taking into account the microturbulence velocity when calculating the spectra of stars in the clusters. The method uses medium-resolution integrated-light spectra of clusters ($\lambda/\delta\lambda \geq 1000$) in a wide spectral range ($\lambda \sim [3900; 5000]$ Å) and, therefore, can be applied not only to the study of Galactic, but also bright extragalactic objects. The choice of the

optimal isochrone for calculating synthetic spectra of clusters is made by matching the shape and intensity of the observed and theoretical Balmer line profiles, as well as by reproducing the observed ratio of the Ca I and Ca II lines.

In this article we demonstrate the agreement of our results for Galactic globular clusters with the corresponding literature values obtained from stellar photometry and spectroscopy of the brightest stars in the objects with high-resolution spectrographs, as well as from the studies of integrated spectra of the clusters. The reasons for the significant deviations of the obtained ages and metallicities of the clusters from the corresponding literature values are discussed in Section 4. The systematic difference between our estimates of $[\text{C}/\text{Fe}]$ and the literature data obtained by spectroscopy of the brightest stars in the objects is interpreted by us as the effect of changes of the chemical composition in the atmospheres of stars during their evolution.

It was shown that the results of our determination of chemical abundances at a given metallicity agree with the corresponding values in the models of chemical evolution by Kobayashi et al. (2006) and Matteucci et al.(2019).

In the future, we plan to study the influence of non-LTE effects on the elemental abundances obtained using integrated-light spectra. Also, we plan to investigate the influence of the stellar mass function on the integrated spectra of clusters.

ACKNOWLEDGMENTS

We thank the anonymous referee for the comments, that allowed us to improve the paper. We thank A. I. Kolbin for help in preparing the figures in Section 3.1 of the article.

FUNDING

The work was supported by the grant RFBR 18-02-00167. Sh. N. N. appreciates the grant

RFBR 18-42-160003. The work of VVSh was partially funded by the subsidy N 0671-2020-0052 to KFU for the scientific activities.

CONFLICT OF INTEREST

The authors declare no conflict of interest regarding this paper.

-
1. G. Bertelli, L. Girardi, P. Marigo, and E. Nasi, *Astron. and Astrophys.* **484** (3), 815 (2008).
 2. E. Bica, S. Ortolani, and B. Barbuy, *Publ. Astron. Soc. Australia* **33**, e028 (2016).
 3. C. Boeche and E. K. Grebel, *Astron. and Astrophys.* **587**, A2 (2016).
 4. C. Boeche, A. Siebert, M. Williams, et al., *Astron. J.* **142** (6), 193 (2011).
 5. K. Brogaard, D. A. VandenBerg, L. R. Bedin, et al., *Monthly Notices Royal Astron. Soc.* **468** (1), 645 (2017).
 6. H. Bruntt, S. Basu, B. Smalley, et al., *Monthly Notices Royal Astron. Soc.* **423** (1), 122 (2012).
 7. I. Cabrera-Ziri, C. Lardo, and A. Mucciarelli, *Monthly Notices Royal Astron. Soc.* **485** (3), 4128 (2019).
 8. A. Calamida, K. C. Sahu, S. Casertano, et al., *Astrophys. J.* **810** (1), 8 (2015).
 9. B. W. Carney, *Star Clusters, Saas-Fee Advanced Courses*, Vol. 28: *Stellar Evolution in Globular Clusters* (Springer-Verlag, Berlin, Heidelberg, 2001) p. 1.
 10. E. Carretta, A. Bragaglia, R. G. Gratton, et al., *Astron. and Astrophys.* **516**, A55 (2010).
 11. F. Castelli and R. L. Kurucz, *IAU Symp.* **210**, A20 (2003).
 12. B. Chaboyer, A. Sarajedini, and T. E. Armandroff, *Astron. J.* **120** (6), 3102 (2000).
 13. G. Chabrier, *Astrophys. Space Sci. Library* **327**, 41 (2005).
 14. C. Charbonnel, *EAS Publ. Ser.* **80–81**, pp. 177–226 (2016).
 15. J. E. Colucci, R. A. Bernstein, and A. McWilliam, *Astrophys. J.* **834** (2), 105 (2017).
 16. C. Conroy, A. Villaume, P. G. van Dokkum, and K. Lind, *Astrophys. J.* **854** (2), 139 (2018).
 17. P. A. Denissenkov, D. A. VandenBerg, G. Kopacki, and J. W. Ferguson, *Astrophys. J.* **849** (2), 159 (2017).
 18. A. Dotter, A. Sarajedini, J. Anderson, et al., *Astrophys. J.* **708** (1), 698 (2010).
 19. D. A. Forbes and T. Bridges, *Monthly Notices Royal Astron. Soc.* **404** (3), 1203 (2010).
 20. G. A. Galazutdinov, V. V. Shimansky, A. Bondar, et al., *Monthly Notices Royal Astron. Soc.*

- 465** (4), 3956 (2017).
21. R. G. Gratton, E. Carretta, and A. Bragaglia, *Astron. Astrophys. Rev.* **20**, 50 (2012).
 22. B. M. S. Hansen, J. S. Kalirai, J. Anderson, et al., *Nature (London)* **500** (7460), 51 (2013).
 23. W. E. Harris, *Astron. J.* **112**, 1487 (1996).
 24. C. I. Johnson, N. Caldwell, R. M. Rich, et al., *Astrophys. J.* **842** (1), 24 (2017).
 25. F. Kahraman Aliçavuş, E. Niemczura, P. De Cat, et al., *Monthly Notices Royal Astron. Soc.* **458** (3), 2307 (2016).
 26. D. A. Khamidullina, M. E. Sharina, V. V. Shimansky, and E. Davoust, *Astrophysical Bulletin* **69** (4), 409 (2014).
 27. C. Kobayashi, H. Umeda, K. Nomoto, et al., *Astrophys. J.* **653** (2), 1145 (2006).
 28. R. P. Kraft, *Publ. Astron. Soc. Pacific* **106**, 553 (1994).
 29. P. Kroupa, C. A. Tout, and G. Gilmore, *Monthly Notices Royal Astron. Soc.* **262**, 545 (1993).
 30. J. M. D. Kruijssen, J. L. Pfeffer, M. Reina-Campos, et al., *Monthly Notices Royal Astron. Soc.* **486** (3), 3180 (2019).
 31. S. S. Larsen, J. P. Brodie, and J. Strader, *Astron. and Astrophys.* **546**, A53 (2012).
 32. S. S. Larsen, J. P. Brodie, and J. Strader, *Astron. and Astrophys.* **601**, A96 (2017).
 33. L. Malavolta, C. Sneden, G. Piotto, et al., *Astron. J.* **147** (2), 25 (2014).
 34. A. F. Marino, S. Villanova, G. Piotto, et al., *Astron. and Astrophys.* **490** (2), 625 (2008).
 35. V. A. Marsakov, V. V. Koval', and M. L. Gozha, *Astrophysical Bulletin* **74** (4), 403 (2019).
 36. D. Massari, A. Mucciarelli, E. Dalessandro, et al., *Monthly Notices Royal Astron. Soc.* **468** (1), 1249 (2017).
 37. F. Matteucci, V. Grisoni, E. Spitoni, et al., *Monthly Notices Royal Astron. Soc.* **487** (4), 5363 (2019).
 38. A. McWilliam and R. A. Bernstein, *Astrophys. J.* **684** (1), 326 (2008).
 39. V. S. Menzhevitski, N. N. Shimanskaya, V. V. Shimansky, and D. O. Kudryavtsev, *Astrophysical Bulletin* **69** (2), 169 (2014).
 40. S. Mészáros, S. L. Martell, M. Shetrone, et al., *Astron. J.* **149** (5), 153 (2015).
 41. T. V. Mishenina, V. E. Panchuk, and N. N. Samus', *Astronomy Reports* **47** (3), 248 (2003).
 42. P. E. Nissen, *Astron. and Astrophys.* **97**, 145 (1981).
 43. A. Pietrinferni, S. Cassisi, M. Salaris, and S. Hidalgo, *Astron. and Astrophys.* **558**, A46 (2013).
 44. G. Piotto, I. R. King, S. G. Djorgovski, et al., *Astron. and Astrophys.* **391**, 945 (2002).
 45. B. J. Pritzl, K. A. Venn, and M. Irwin, *Astron. J.* **130** (5), 2140 (2005).
 46. J. C. Roediger, S. Courteau, G. Graves, and R. P. Schiavon, *Astrophys. J. Suppl.* **210** (1), 10 (2014).
 47. E. E. Salpeter, *Astrophys. J.* **121**, 161 (1955).
 48. N. C. Santos, S. G. Sousa, A. Mortier, et al., *Astron. and Astrophys.* **556**, A150 (2013).
 49. A. Sarajedini, L. R. Bedin, B. Chaboyer, et al., *Astron. J.* **133** (4), 1658 (2007).
 50. M. Schaeuble, G. Preston, C. Sneden, et al., *Astron. J.* **149** (6), 204 (2015).
 51. R. P. Schiavon, J. A. Rose, S. Courteau, and L. A. MacArthur, *Astrophys. J. Suppl.* **160** (1), 163 (2005).
 52. D. J. Schlegel, D. P. Finkbeiner, and M. Davis, *Astrophys. J.* **500** (2), 525 (1998).
 53. M. E. Sharina, C. J. Donzelli, E. Davoust, et al., *Astron. and Astrophys.* **570**, A48 (2014).

54. M. E. Sharina and V. V. Shimansky, IAU Symp. **351**, pp. 165–169 (2020).
55. M. E. Sharina, V. V. Shimansky, and E. Davoust, Astronomy Reports **57** (6), 410 (2013).
56. M. E. Sharina, V. V. Shimansky, and D. A. Khamidullina, Astrophysical Bulletin **73** (3), 318 (2018).
57. M. E. Sharina, V. V. Shimansky, and A. Y. Kniazev, Monthly Notices Royal Astron. Soc. **471** (2), 1955 (2017).
58. M. E. Sharina and V. V. Shimansky, arXiv:2004.05957 (2020).
59. J. D. Simpson, S. L. Martell, and C. A. Navin, Monthly Notices Royal Astron. Soc. **465** (1), 1123 (2017).
60. V. Testa, C. E. Corsi, G. Andreuzzi, et al., Astron. J. **121** (2), 916 (2001).
61. D. A. VandenBerg, K. Brogaard, R. Leaman, and L. Casagrande, Astrophys. J. **775** (2), 134 (2013).
62. D. Yong, A. Alves Brito, G. S. Da Costa, et al., Monthly Notices Royal Astron. Soc. **439** (3), 2638 (2014).

Translated by Sharina M.E.

